RSC Advances



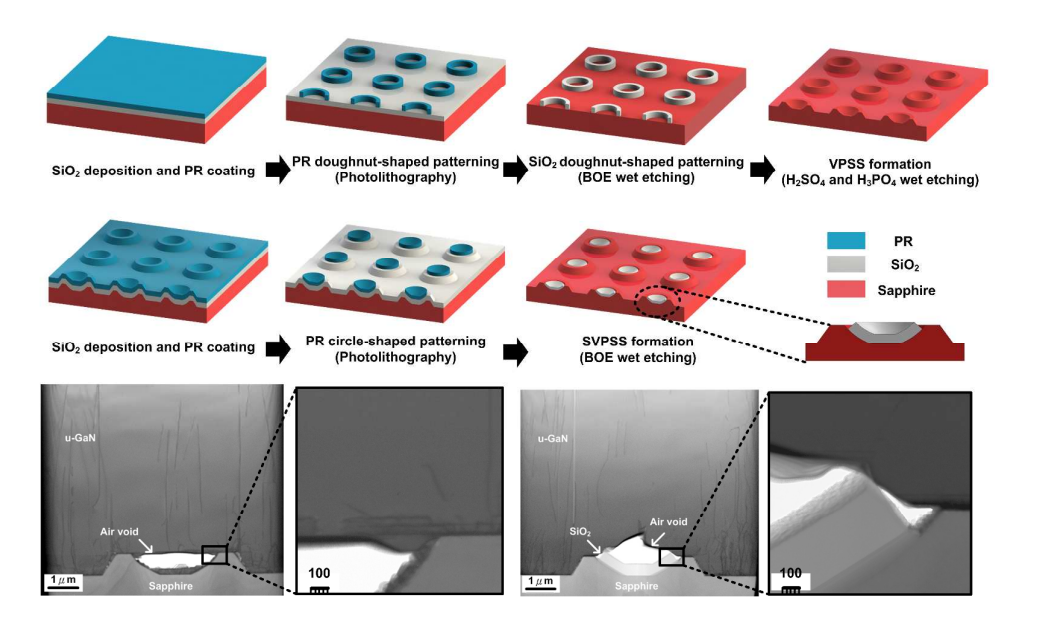
This is an *Accepted Manuscript*, which has been through the Royal Society of Chemistry peer review process and has been accepted for publication.

Accepted Manuscripts are published online shortly after acceptance, before technical editing, formatting and proof reading. Using this free service, authors can make their results available to the community, in citable form, before we publish the edited article. This Accepted Manuscript will be replaced by the edited, formatted and paginated article as soon as this is available.

You can find more information about *Accepted Manuscripts* in the **Information for Authors**.

Please note that technical editing may introduce minor changes to the text and/or graphics, which may alter content. The journal's standard <u>Terms & Conditions</u> and the <u>Ethical guidelines</u> still apply. In no event shall the Royal Society of Chemistry be held responsible for any errors or omissions in this *Accepted Manuscript* or any consequences arising from the use of any information it contains.







Journal Name

ARTICLE

Received 00th January 20xx, Accepted 00th January 20xx

DOI: 10.1039/x0xx00000x

www.rsc.org/

Enhanced performance of InGaN-based light-emitting diodes grown on volcano-shaped patterned sapphire substrates with embedded SiO₂

Yao-Hong You, Fu-Chuan Chu, Han-Cheng Hsieh, Wen-Hsin Wu, Ming-Lun Lee, Chieh-Hsiung Kuan and Ray-Ming Lin

This paper describes highly efficient InGaN-based light-emitting diodes (LEDs) grown on volcano-shaped patterned sapphire substrates with embedded SiO₂ (SVPSS). Raman spectroscopy and transmission electron microscopy revealed that the LEDs grown on the SVPSS had high internal quantum efficiency resulting from relaxed compressive strain and fewer threading dislocations in the GaN epitaxial layers. Experimentally measured data and ray-tracing simulations suggested that the enhancement in the light extraction efficiency was due to the light scattering effect arising from the conical air voids and the gradual refractive index matching resulting from the embedded SiO₂. Compared with a conventional LED operated at an injection current of 350 mA, the light output power from our LED grown on the SVPSS was increased by 72%.

Introduction

In recent years, InGaN-based light-emitting diodes (LEDs) have found widespread applicability as backlights in flat-panel displays and in solid state lighting. Although InGaN-based LEDs are commercially available, there remains room for improvement in their external quantum efficiency (EQE). Two factors determine the EQE of an InGaN-based LED: the internal quantum efficiency (IQE) and the light-extraction efficiency (LEE). A low IQE can arise from low crystal quality of the epitaxial GaN layer and strong polarization-induced electric fields in the InGaN/GaN multiple quantum wells (MQWs). A high density of dislocations (10⁸–10¹⁰/cm²) in the epitaxial GaN layers is inevitable because of the large lattice mismatch and the different thermal expansion coefficients between the epitaxial GaN layer and the sapphire substrate. If these dislocations propagated to the surface, these dislocations can deteriorate the performance of optical and electronic devices. Moreover, even if the IQE is close to unity, the LEE is still poor as a result of total internal reflection between the semiconductor and the outer medium. Considering the refractive indices of GaN (n = 2.4) and air (n = 1), the critical angle for total internal reflection at the GaN-air interface is merely 23°, severely restricting the LEE of InGaN-based LEDs.¹

Fig. 1 Schematic representation of the fabrication of (a) VPSS and (b) SVPSS structures.

Electronic Supplementary Information (ESI) available: [details of any supplementary information available should be included here]. See DOI: 10.1039/x0xx00000x

Many methods have been proposed to improve the EQE of InGaN-based LEDs, including the use of patterned sapphire substrates (PSSs), $^{2-5}$ epitaxial lateral overgrowth (ELOG), $^{6-8}$ surface structures, $^{9-11}$ semi/non-polar QWs, 12,13 and nanoporous GaN. 14,15 Among these technologies, the PSSs method is currently being used in manufacturing industries because of its high production yield. The PSSs technique can improve both IQE and LEE by decreasing threading dislocations and enhancing light scattering. The light output power (LOP) of InGaN-based LEDs is dependent on the shape of its PSS. The LEE of GaN-based LEDs grown on a volcano-shaped patterned sapphire substrate (VPSS) was reportedly to be better than that grown on hemispherical PSS, due to the more-faceted sidewalls. 16 Recently, Lin et al. 17 reported that the LOPs of InGaN-based LEDs grown on SiO₂-PSS were enhanced compared with those grown on PSS because of the lower threading dislocation density (TDD) and because the refractive index of SiO₂ is lower than that of sapphire. Nevertheless, the growth of epitaxial GaN layers on a SiO₂-PSS, especially a highly ordered one, requires complex epitaxy techniques to enhance the lateral overgrowth, thereby limiting the rate of

SiO, deposition and PR coating

PR doughnut-shaped patterning

SiO, deposition and PR coating

PR doughnut-shaped patterning

(BOE wet etching)

VPSS formation

(H₃SO₄ and H₃PO₄ wet etching)

PR

SiO₂
Sapphire

^{a.} Graduate Institute of Electronics Engineering, Department of Electrical Engineering, National Taiwan University, Taipei, 10617, Taiwan.

^{b.} Graduate Institute of Electronic Engineering and Green Technology Research Center, Chang Gung University, Tao-Yuan, 333, Taiwan. E-mail: rmlin@mail.cgu.edu.tw

ARTICLE Journal Name

growth of the epitaxial GaN layer. ^{18,19} Accordingly, there is much room for improvement for lowering the costs of growing epitaxial layers in commercial manufacturing.

In this paper, we report high-performance InGaN-based light-emitted diodes grown on volcano-shaped patterned sapphire substrates with embedded SiO₂ (SVPSS). We found experimentally that the residual compressive strain and total internal reflection could both be suppressed as a result of the embedded conical air void array in the GaN epitaxial layer formed through ELOG using embedded SiO₂. We describe herein the geometric morphologies, electrical properties, and optical characteristics of these LED structures.

Experimental

The VPSS and SVPSS structures were fabricated using photolithography and wet-etching technology. Figure 1(a) illustrates the processing steps involved in the fabrication of the VPSS structures. Briefly, the fabrication began with plasma-enhanced chemical vapor deposition of a 240-nm SiO₂ film on a 2-inch c-plane sapphire substrate. Next, the SiO₂ film was coated with photoresist (PR) and then doughnut-shaped PR mask array patterns were formed on the SiO₂ film using photolithography. After removal of the PR, the doughnutshaped PR mask array patterns were transferred to the SiO₂ film using a buffered oxide etchant (BOE). The sapphire substrate presenting the doughnut-shaped SiO₂ hard mask was etched in a H_2SO_4/H_3PO_4 (3:1) solution at 250 °C. Finally, the residual doughnut-shaped SiO₂ hard mask was removed through BOE etching to obtain the VPSS. Figure 1(b) displays the fabrication of an SVPSS structure. Based on the fabrication of the VPSS, a 240-nm-thick SiO₂ film was deposited, through plasma-enhanced chemical vapor deposition, as an interlayer on top of the VPSS. Using a photolithographic alignment technique, circle-shaped PR mask array patterns were defined in the centers of the volcanos. The circle-shaped PR mask array patterns were transferred to the 240-nm SiO₂ film through BOE etching and the residual PR was removed using acetone. Using this approach, SVPSS structures were formed on the 2inch c-plane sapphire substrates. The surface morphologies, periodicities, heights, and diameters of the features of these VPSS and SVPSS structures were examined using an FEI Dual-Beam NOVA 600i Focused Ion Beam [Figures 2(a) and (b)]. The volcano patterns had a diameter of 5 μm, a height of 400 nm, and a periodicity of 9 µm on the 2-inch c-plane sapphire

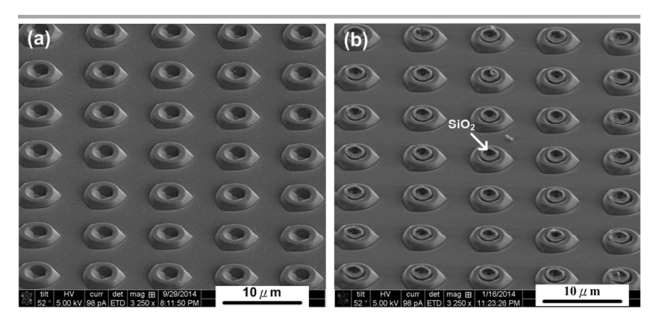


Fig. 2 SEM images of (a) VPSS and (b) SVPSS structures.

substrate.

After a sample cleaning process, InGaN-based LED samples were grown on the PSSs through atmospheric-pressure metal organic chemical vapor deposition (AP-MOCVD; Taiyo Nippon Sanso SR2000) under three-flow gas injection. Prior to the growth process, the substrate was thermally baked at 1180 °C in H₂ gas to remove any surface contaminants. The InGaNbased LED structures, comprising a 25-nm-thick low-GaN nucleation layer, a 2.5-µm-thick temperature unintentionally doped GaN buffer layer (grown at 1180 °C), and a 3-µm-thick n-GaN layer, using SiH4 as the n-type dopant, were first grown on the PSSs. Seven pairs of InGaN/GaN MQWs having a 3-nm-thick InGaN well and a 11-nm-thick GaN barrier (grown at 800 and 850 °C, respectively) were then deposited, followed by a 20-nm-thick p-AlGaN electron blocking layer and a 120-nm-thick p-GaN layer, using Cp₂Mg as the p-type dopant. InGaN-based LEDs were grown on a conventional sapphire substrate (CSS), the VPSS, and the SVPSS under the same growth conditions without employing a recovery technique, which can significantly increase the cost to fabricating InGaN-based LEDs.

Results and Discussion

We employed transmission electron microscopy (TEM) to investigate the crystalline quality of the GaN epitaxial layers grown on the VPSS and SVPSS. Figures 3(a) and 3(c) reveal that the TDDs in the lateral overgrowth GaN region grown on the SVPSS were less than those grown on the VPSS. Figure 3(b) indicates that GaN could grow from the $\left\{1\,\overline{1}\,08\right\}$ facet of the sapphire on inside the volcano structures, causing TDDs from the coalescing boundary between two adjacent GaN domains. The SiO2 inserted into the volcano structures could, however, sufficiently suppress GaN growth therein, as observed in Figure

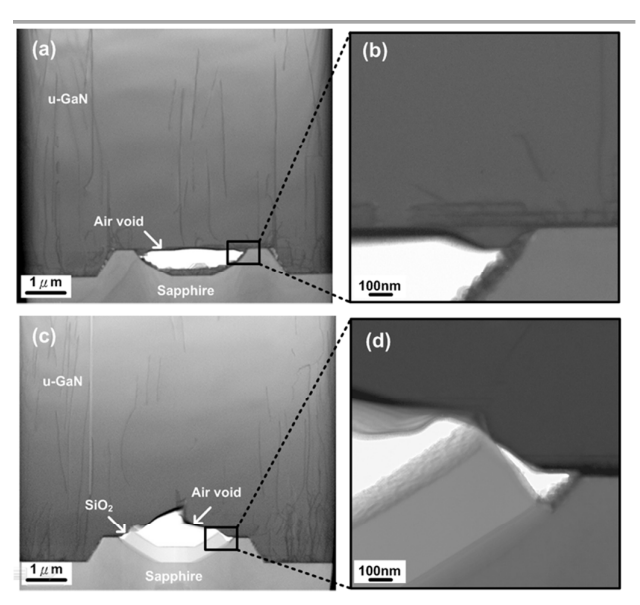


Fig. 3 TEM images of InGaN-based LEDs grown on (a, b) VPSS and (c, d) SVPSS structures

Journal Name ARTICLE

3(d). Hence, the SVPSS could improve the GaN crystal quality. In addition to TEM, we also used X-ray diffraction (XRD) to evaluate the GaN quality. The full widths at half-maximum (FWHMs) of the (0 0 2) GaN for the InGaN-based LEDs grown on the CSS, VPSS, and SVPSS were 277, 295, and 252 arcsec, respectively; those of the (1 0 2) GaN were 360, 298, and 298 arcsec, respectively. The FWHM of the (0 0 2) GaN for the InGaN-based LED grown on the VPSS was 18 arcsec larger than that grown on the CSS. However, the FWHM of the (1 0 2) GaN for the InGaN-based LED grown on the VPSS was 52 arcsec smaller than that grown on the CSS. It had reported that the FWHMs of (0 0 2) GaN and (1 0 2) GaN are proportional to the screw and edge dislocation.²¹ This indicated that the InGaNbased LED grown on the VPSS mainly improved edge dislocation and slightly degraded screw dislocation. The total dislocation density in the InGaN-based LED with VPSS was lower than that InGaN-based LED with CSS. Furthermore, our designed SVPSS could effectively alleviate TDDs and improve the epitaxial quality, in good agreement with the XRD data and TEM images.

After epitaxial growth, we characterized the samples using the constant-excitation power of a micro-Raman (μ -Raman) system to compare the strain in the GaN epitaxial layers. Figure 4 displays the room-temperature Raman spectra of the E₂(high) phonon mode of the GaN epitaxial layers grown on the CSS, VPSS, and SVPSS. The Raman shifts of the E₂(high) mode of the GaN epitaxial layers grown on the CSS, VPSS, and SVPSS were 570.57, 571.13, and 570.24 cm⁻¹, respectively. The E₂(high) phonon frequency of perfect GaN at room-temperature is 567.6 cm⁻¹. 22 thus, the residual strain can be calculated from the measured E₂(high) mode Raman shift using the expression 23

$$\varepsilon_{xx} = \sigma_{xx} \cdot \frac{1}{M_f} = \left(\frac{\Delta \omega}{K}\right) \cdot \frac{1}{M_f} \tag{1}$$

where ε_{xx} and σ_{xx} represent the residual strain and residual stress, respectively, in the GaN epitaxial layers; $M_{\rm f}$ is the biaxial modulus ($M_f=449.6{\rm GPa}$) and K is the proportionality factor ($K=4.2{\rm cm}^{-1}{\rm GPa}^{-1}$) for GaN; and $\Delta\omega$ is the Raman shift of the

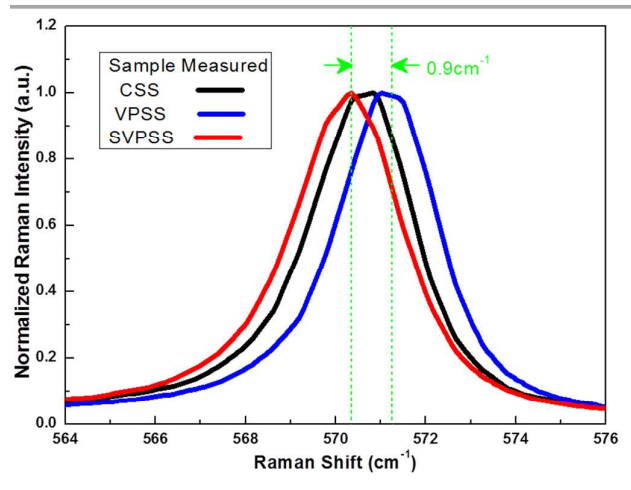


Fig. 4 Room-temperature Raman spectra of GaN epitaxial layers grown on the CSS, VPSS, and SVPSS structures.

E₂(high) phonon frequency with respect to perfect GaN. The associated residual strains calculated for the InGaN-based LEDs grown on the CSS, the VPSS, and the SVPSS were -1.57×10^{-3} , -1.87×10^{-3} , and -1.4×10^{-3} , respectively. These negative values indicate that the residual strain was compressive. The residual compressive strain originated mainly from the large lattice mismatch between the sapphire substrates and the GaN epitaxial layers. The InGaN-based LED grown on the VPSS had residual compressive strain higher than that grown on the CSS. From the previous study published by our group, 2,24 the residual compressive strain in the GaN epitaxial layer was determined by PSSs with various periodic patterns. By designing the VPSS with embedded SiO₂, the conical air voids can be formed naturally because the GaN during the ELOG process needed to climb over a lip of SiO₂. To further elucidate the effect of the conical air void, we estimated that the surface area between GaN and air void of the SVPSS was 30% higher than that of the VPSS. The large area of the conical air void can decrease the residual compressive strain. 14,25 Therefore, the residual compressive strain in the GaN epitaxial layer grown on the SVPSS was more relaxed than that on the VPSS.

To verify the smaller QCSE of InGaN-based LEDs grown on the SVPSS within the InGaN/GaN MQWs acquired by the smaller compressive, excitation power dependent PL measurement²⁶ was carried out for understanding the QCSE. Figure 5 shows the peak wavelength shifts of the PL spectrum under different excitation power density for the InGaN-based LEDs with the CSS, VPSS, and SVPSS from 7.9×10^2 to 2.4×10^3 W/cm². Based on the screening effect of QCSE, we focused on the PL spectra of InGaN-based LEDs having the CSS, VPSS, and SVPSS at the excitation power density of 7.9×10^2 and 2.4×10^3 W/cm² as shown the insets of Figure 5, respectively. From these spectra, the shifts in PL peak wavelength for the InGaN-based LEDs with CSS, VPSS and SVPSS were 3.4, 4.2 and 2.2 nm, respectively. The small shifts in PL peak wavelength for the InGaN-based LEDs grown on the SVPSS can be reasoned by observing the weaker action of the QCSE resulting from the relaxation of the GaN epitaxial layer. The abatement of

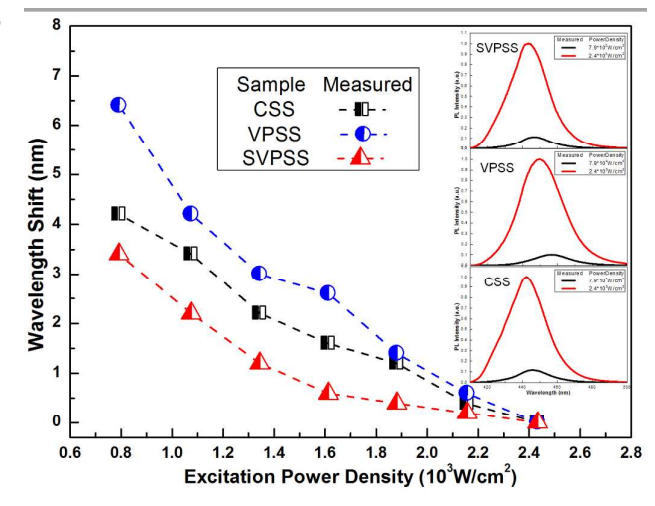


Fig. 5 QCSE phenomenon of InGaN-based LEDs grown on the CSS, VPSS, and SVPSS structures.

ARTICLE Journal Name

QCSE within the MQWs can increase overlap between electron and hole wave functions and consequently result in a stronger radiative recombination rate. To confirm the improvement of the IQE, the relative IQEs of InGaN-based LEDs grown on the CSS, VPSS, and SVPSS were conducted by temperature-dependent PL (TD-PL) system, assuming the IQE is 100% at a low temperature of 20K. The relative IQEs of the InGaN-based LEDs grown on the CSS, VPSS, and SVPSS were 22, 24, and 31%, respectively. The IQE of InGaN-based LEDs grown on the CSS and VPSS were similar because the InGaN-based LED with VPSS had better GaN crystalline quality but had larger QCSE. Moreover, the InGaN-based LED grown on the SVPSS had the highest IQE because of a significant relaxation of residual compressive strain and reduction of TDDs within the InGaN/GaN MQWs.

Figure 6 displays the far-field radiation patterns of the InGaN-based LEDs grown on the CSS, VPSS, and SVPSS, as analyzed through angle-resolved EL measurements at an injection current of 100 mA. At all detection angles, the light output intensity (LOI) of the InGaN-based LED grown on the SVPSS was higher than that of the InGaN-based LED grown on the VPSS. Furthermore, in the normal direction (θ = 90°), the LOIs of the InGaN-based LEDs grown on the VPSS and SVPSS were 40 and 85% higher, respectively, than that of the InGaN-based LED grown on the CSS. This observation implies that light trapped in the LED featuring the SVPSS structure was scattered upward by the conical air voids and the embedded SiO₂.

To gain greater insight into the influence of the embedded SiO_2 and the conical air voids on the LEEs of our InGaN-based LEDs, we performed Trace-Pro ray-tracing simulations to calculate the light extraction from each face of the InGaN-based LEDs. As depicted in Figure 7(a), we placed six different receivers as close as possible to the GaN side face (GaN-Side), the sapphire side face (Sapphire-Side), and the four side face (4-Side) of the LED structures. The LED structures considered for the simulations were as similar as possible to the real LED structures; we assumed that 2000 light rays at a power of 2 W were generated randomly within the active region. The LEE of unencapsulated LEDs with CSS, VPSS, and SVPSS were 27, 55, and 59%, respectively. To clearly identify the principle behind the improvement in light extraction induced by the embedded SiO_2 and conical air voids,

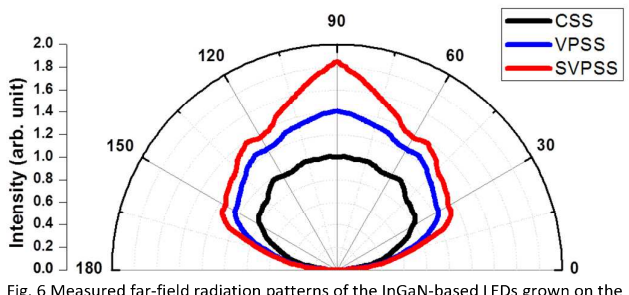


Fig. 6 Measured far-field radiation patterns of the InGaN-based LEDs grown on the CSS, VPSS, and SVPSS structures.

the percentage increase in light intensity was defined as that from the InGaN-based LED grown on the SVPSS divided by that from the InGaN-based LED grown on the VPSS. Figure 7(b) displays the light intensities and percentage increases for InGaN-based LEDs constructed on the VPSS and SVPSS, detected using the various detectors. The simulations revealed only slight percentage increases in the light intensities on the Sapphire-Side and 4-Side, but a significant percentage increase on the GaN-Side. Thus, the conical air voids could efficiently change the light path in an upward direction, improving the light extraction of the LEDs as a result of the large difference in refractive index at the air-GaN interface and the slanted angle of the conical air voids.²⁸ Furthermore, the embedded SiO₂ helped to decrease the refractive index mismatch between the GaN and air, thereby improving the LEE when the light was trapped in the conical air voids.

Figure 8 presents the current–voltage (I–V) characteristics and the LOPs of the InGaN-based LEDs, fabricated using the standard industrial $1 \times 1 \text{ mm}^2$ LED die process. The forward voltages of the InGaN-based LEDs grown on the CSS, VPSS, and SVPSS at an injection current of 350 mA were 3.48, 3.51, and 3.47 V, respectively. The plots of forward current with respect to voltage for the InGaN-based LEDs grown on the CSS, VPSS, and SVPSS were very similar. The LOPs for the InGaN-based LEDs grown on the CSS, VPSS, and SVPSS at a current of 350 mA were 192, 270, and 331 mW, respectively. Compared with the InGaN-based LED grown on the CSS at an injection current of 350 mA, the LOPs of the samples grown on the VPSS and SVPSS were enhanced by 40 and 72%, respectively. From above analyses, the InGaN-based LED with the VPSS had a higher output power than the InGaN-based LED with the CSS, which is mainly attributed to the light scattering effect by VPSS and embedded air voids. Furthermore, the LOP of the InGaNbased LED grown on the SVPSS was higher than that grown on the VPSS. Our simulations and experimental results suggest that the stronger LOP for the sample grown on the SVPSS arose from the fewer dislocations in the GaN epitaxial layers, the lower QCSE acquired by the smaller residual compressive strain in the GaN epitaxial layers, and the higher LEE arising from the effects of light scattering from conical air voids and gradual refractive index matching by the embedded SiO₂.

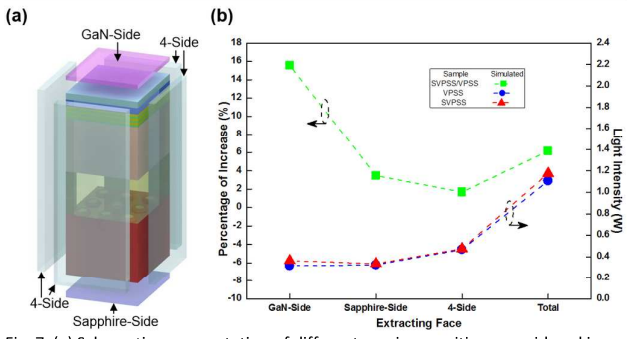


Fig. 7 (a) Schematic representation of different receiver positions considered in the simulation. (b) Light intensity and percentage increase in light intensity of InGaN-based LEDs grown on the VPSS and SVPSS, detected at the various detectors.

Journal Name ARTICLE

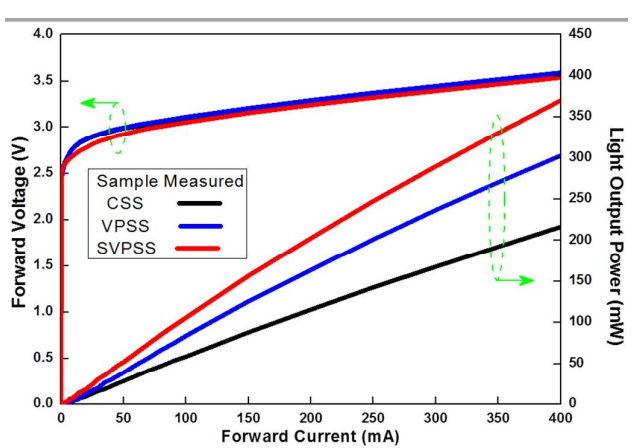


Fig. 8 LOP-I–V curves of InGaN-based LEDs grown on CSS, VPSS, and SVPSS, plotted with respect to the forward current.

Conclusions

The growth of InGaN-based LEDs on SVPSS structures featuring conical air voids can suppress the compressive strain in GaN epitaxial layers and improve the LEE. Experimentally measured data and ray-tracing simulations confirmed that the relaxation of the compressive stain within the corresponding epitaxial layers resulted from the relatively large volume of the conical air voids, while the enhancement in LEE arose predominantly from the significant increase in light extraction through the GaN face as a result of the presence of the conical air voids. At an injection current of 350 mA, the values of the LOP from the InGaN-based LEDs grown on the VPSS and SVPSS were 40 and 72% greater, respectively, that that of the corresponding LED grown on the CSS.

Acknowledgements

This work was supported by the National Science Council of Taiwan (project no. NSC 103-2221-E-182-018) and in part by Sino American Silicon Products Incorporation

Notes and references

- 1 S. Noda, M. Fujita, Nat. Photonics., 2009, **3**, 129–130.
- V. C. Su, P. H. Chen, R. M. Lin, M. L. Lee, Y. H. You, C. I. Ho, Y. C. Chen, W. F. Chen, C. H. Kuan, *Optics Express*, 2013, 21, 30065–30073.
- 3 J. H. Cheng, Y. S. Wu, W. C. Liao, B. W. Lin, Appl. Phys. Lett., 2010, 96, 051109.
- 4 Y. H. You, V. C. Su, T. E. Ho, B. W. Lin, M. L. Lee, A. Das, W. C. Hsu, C. H. Kuan, R. M. Lin, *Nanoscale Res. Lett.*, 2014, 9, 596.
- 5 X.-H. Huang, J.-P. Liu, J.-J. Kong, H. Yang, H.-B. Wang, Opt. Express, 2011, 19, A949–A955.
- S. Nakamura, M. Senoh, S. I. Nagahama, N. Iwasa, T. Yamada, T. Matsushita, H. Kiyoku, Y. Sugimoto, T. Kozaki, H. Umemoto, M. Sano, K. Chocho, *Appl. Phys. Lett.*, 1998, 72, 211–213.
- 7 S. Nakamura, *Science*, 1998, **281**, 956–961.
- C. Bayram, J. L. Pau, R. McClintock, M. Razeghi, Appl. Phys., 2009, B95, 307–314.
- 9 J. J. Wierer, A. David, M. M. Megens, Nat. Photonics, 2009, 3, 163–169.
- B. Sun, L. Zhao, T. Wei, X. Yi, Z. Liu, G. Wang, J. Li, F. Yi, Opt. Express, 2012, 20, 18537–18544.

- 11 M. L. Lee, Y. H. You, R. M. Lin, C. J. Hsieh, V. C. Su, P. H. Chen, C. H. Kuan, *IEEE Photonics.*, 2014, 6, 8200408.
- 12 P. Waltereit, O. Brandt, A. Trampert, H. T. Grahn, J. Menniger, M. Ramsteiner, M. Reiche, K. H. Ploog, *Nature*, 2000, 406, 865–868.
- 13 H. Masui, S. Nakamura, S. P. DenBaars, U. K. Mishra, IEEE Trans. Electron. Dev., 2010, 57, 88–100.
- 14 K. J. Lee, S. J. Kim, J. J. Kim, K. Hwang, S. T. Kim, S. J. Park, Opt. Express, 2014 22, A1164–A1173.
- 15 H. Hartono, C. B. Soh, S. Y. Chow, S. J. Chua, E. A. Fitzgerald, Appl. Phys. Lett., 2007, 90, 171917.
- 16 J. B. Kim, S. M. Kim, Y. W. Kim, S. K. Kang, S. R. Jeon, N. Hwang, Y. J. Choi, C. S. Chung, Jpn. J. Appl. Phys., 2010, 49, 042102.
- 17 D. W. Lin, J. K. Huang, C. Y. Lee, R. W. Chang, Y. P. Lan, C. C. Lin, K. Y. Lee, C. H. Lin, P. T. Lee, G. C. Chi. J. Display Technol., 2013. 9, 285–291.
- D. Kapolnek, S. Keller, R. Vetury, R. D. Underwood, P. Kozodoy, S. P. DenBaars,
 U. K. Mishra, Appl. Phys. Lett., 1997, 71, 1204–1206.
- K. Hiramatsu, K. Nishiyama, M. Onishi, H. Mizutani, M. Narukawa, A. Motogaito, H. Miyake, Y. Iyechika, T. Maeda, J. Cryst. Growth., 2000, 221, 316–326
- S. X. Jiang, Z. Z. Chen, X. Z. Jiang, X. X. Fu, S. Jiang, Q. Q. Jiao, T. J. Yu G. Y. Zhang, CrystEngComm, 1998, 58, 12899–12907.
- 21 B. Heying, X. H. Wu, S. Keller, Y. Li, D. Kapolnek, B. P. Keller, S. P. DenBaars, J. S. Speck, Appl. Phys. Lett. 1996, 68, 643.
- 22 V. Y. Davydov, Y. E. Kitaev, I. N. Goncharuk, A. N. Smirnov, J. Graul, O. Semchinova, D. Uffmann, M. Smirnov, A. Mirgorodsky, R. Evarestov, *Phys. Rev.*, 1998, **B58**, 12899–12907.
- 23 S. Hearne, E. H. Chason, J. A. Floro, J. Figiel, J. Hunter, H. Amano, I. S. T. Tsong, Appl. Phys. Lett., 1999, 74, 356.
- 24 P. H. Chen, V. C. Su, Y. H. You, M. L. Lee, C. J. Hsieh, C. H. Kuan, H. M. Chen, H. B. Yang, H. C. Lin, R. M. Lin, F. C. Chu, G. Y. Su, Conference on Lasers and Electro-Optics, 2013, CM4F.8
- J. Kim, H.j. Woo, K. Joo, S. Tae, J. Park, D. Moon, S.H. Park, J. Jang, Y. Cho, J. Park, H. Yuh, G. Lee, I. Choi, Y. Nanishi, H.N. Han1, K. Char, E. Yoon, Sci. Rep., 2013, 3, 3201.
- 26 H. Yu, L. K. Lee, T. Jung, P. C. Ku, Appl. Phys. Lett., 2007, 90, 141906.
- S. Watanabe, N. Yamada, M. Nagashima, Y. Ueki, C. Sasaki, Y. Yamada, T. Taguchi, K. Tadatomo, H. Okagawa, H. Kudo, Appl. Phys. Lett., 2003, 83, 4906.
- 28 T.-X. Lee, K.-F. Gao, W.-T. Chien, C.-C. Sun, Opt. Express, 2007, **15**, 6670–6676.